THE JOURNAL OF PHYSICAL CHEMISTRY B

Article

Cite This: J. Phys. Chem. B 2018, 122, 5147−5153

pubs.acs.org/JPCB

Phosphorescence Kinetics of Singlet Oxygen Produced by Photosensitization in Spherical Nanoparticles. Part I. Theory

Andrej Hovan,[†] Shubhashis Datta,[‡] Sergei G. Kruglik,[§] Daniel Jancura,[†,‡] Pavol Miskovsky,[†,‡] and Gregor Bánó*[,†,‡]

[†]Department of Biophysics, Faculty of Science, and [‡]Center for Interdisciplinary Biosciences, Technology and Innovation Park, P. J. Šafárik University, Jesenná 5, 041 54 Košice, Slovak Republic

[§]Laboratoire Jean Perrin, Sorbonne Universités, UPMC Univ. Paris 6, CNRS UMR 8237, 4 Place Jussieu, 75005 Paris, France

Supporting Information

ABSTRACT: The singlet oxygen produced by energy transfer between an excited photosensitizer (pts) and ground-state oxygen molecules plays a key role in photodynamic therapy. Different nanocarrier systems are extensively studied to promote targeted pts delivery in a host body. The phosphorescence kinetics of the singlet oxygen produced by the short laser pulse photosensitization of pts inside nanoparticles is influenced by singlet oxygen diffusion from the particles to the surrounding medium. Two theoretical models are presented in this work: a more complex numerical one and a simple analytical one. Both the models predict the time course of singlet oxygen concentration inside and outside of the spherical particles following short-pulse excitation of pts. On the basis of the comparison of the numerical and analytical results, a semiempirical analytical formula is derived to calculate the characteristic diffusion time of singlet oxygen from the nanoparticles to the surrounding solvent. The phosphorescence intensity of singlet oxygen produced in pts-loaded nanocarrier systems can be calculated as a linear combination of the two concentrations (inside and outside the particles), taking the different phosphorescence emission rate constants into account.

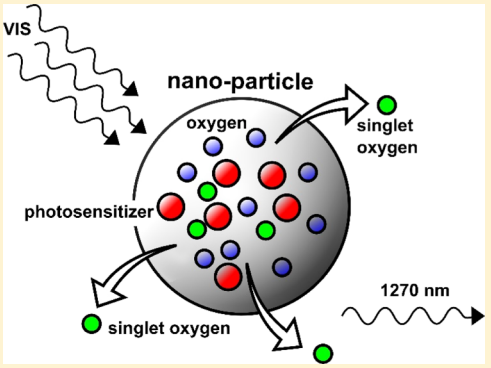

INTRODUCTION

The oxidative stress induced by singlet oxygen in living cells plays a key role in the photodynamic therapy (PDT) of cancer.[1−4] Photosensitive molecules (photosensitizers, pts) internalized into the tumor tissue are used in the PDT to produce singlet oxygen in a cascade of photochemical processes triggered by light absorption. First, an excited singlet state of the pts is created, the energy of which is transferred to a long-lived pts triplet state. Next, the triplet-state pts reacts with the ground-state molecular oxygen to form the singlet oxygen. The chemical processes induced by intracellular singlet oxygen lead to cell death (apoptosis or necrosis) and at the final stage to the destruction of the tumor tissue. The produced singlet oxygen state ($O_2(^1\Delta_g)$) can be detected by monitoring its phosphorescence at 1270 nm. This is usually performed by time-resolved phosphorescence measurements using pulsed laser excitation.[5−14]

During the last decades, various nanoformulations have been developed to promote the targeted delivery of pts in the host body.[15] The properties of pts molecules embedded in different polymer-based nanoparticles,[16−21] protein conjugates,[22] silica-based nanostructures,[23−27] liposomes,[28,29] lipoproteins,[30−32] solid lipid particles,[33] or encapsulated into macrocycles[34,35] were investigated. Another set of scientific papers deal with singlet oxygen generation inside proteins, mostly in LOV-derived flavoprotein systems called mini singlet oxygen generator[36,37] and singlet oxygen photosensitizing protein,[38,39] but also in Zn-substituted myoglobin.[40]

Generally, two strategies can be followed while studying pts molecules (or photoactive sites) located/loaded inside nanoparticles. Either the pts molecules are released from the carrier prior to photoactivation in the target cell or are encapsulated inside the nanoparticle throughout the PDT process. In this case, singlet oxygen created in the nanocarrier interior diffuses out of the particle into the intracellular or extracellular space.

The singlet oxygen lifetime values (τ_Δ) are influenced by the local environments in the particle interior and exterior through the local unimolecular (pseudo-first-order) rate constants of singlet oxygen radiative and nonradiative deactivation: $1/\tau_\Delta = k_r + k_{nr}$. The effect of the environment on k_r and k_{nr} has been studied extensively, mostly for the case of different solvents.[41−44] In heterogeneous systems, the diffusive transport of singlet oxygen through different environments may affect its lifetime in a relatively complicated way, which has an impact on the kinetics of its phosphorescence emission.

Oxygen and singlet oxygen diffusion in pts-loaded heterogeneous polymer systems and phase-separated liquids was monitored by Ogilby and coworkers using time-resolved and

Received: January 19, 2018
Revised: March 29, 2018
Published: April 30, 2018

DOI: 10.1021/acs.jpcb.8b00658
J. Phys. Chem. B 2018, 122, 5147−5153

spatially resolved singlet oxygen phosphorescence measurements.[45,46] Comprehensive analytical and numerical modeling was applied to describe the observed singlet oxygen diffusion.

A numerical model simulating the generation, diffusion, and deactivation of singlet oxygen produced by photosensitization inside the membrane of water-suspended small unilamellar vesicles was reported by Hackbarth and Röder.[47] The experimentally determined time course of singlet oxygen luminescence (following short-pulse excitation) was well-reproduced by this model. The rate constant of radiative depopulation of singlet oxygen was found to be higher (by a factor of 3[47] or 11[48]) inside the lipid bilayer as compared to the aqueous surroundings. It was shown that singlet oxygen diffused out of lipid membranes and spent most of its time in the aqueous environment.

A comprehensive analytical model describing the phosphorescence kinetics of singlet oxygen generated in the protein matrix of Zn-substituted myoglobin has been published by Lepeshkevich and coworkers.[40] The model gives the time course of singlet oxygen concentration inside and outside the protein in a form of analytical formulae. The physical parameters (mostly the rate constants) of the photochemical processes involved in the photosensitization have been determined by fitting the modeling results to the experimental data.

The main goal of the present work is to describe the phosphorescence kinetics of singlet oxygen produced by photosensitization inside solid nanospheres of different radii and composition. Two theoretical models are presented: a more complex numerical one and a simple analytical one. Both models predict the concentration of singlet oxygen inside and outside the particles following short-pulse (nanosecond or sub-nanosecond range) excitation of pts. The particle interior and the surrounding solvent are characterized with singlet oxygen diffusion coefficients, lifetimes, and the corresponding partition coefficient values, which serve as the input parameters of the models. In general, both models can be applied to predict the phosphorescence kinetics of singlet oxygen produced in different nanocarrier/pts combinations. The models are used in part II of the present work (DOI: 10.1021/acs.jpcb.8b00659) to analyze singlet oxygen production by photosensitization of hypericin-loaded LDL particles.

The presented numerical model (analogous to the one developed by Hackbarth and Röder for vesicles[47]) calculates the whole spatiotemporal concentration distribution of singlet oxygen created inside of the nanospheres. The diffusion equation complemented by source and decay terms is solved numerically using finite difference techniques. The model allows for nonhomogeneous material properties and pts distribution to be taken into account inside the nanoparticles. A detailed explanation of the model assumptions and the calculation procedure are provided.

The analytical model is derived for solid spheres with homogeneous interior. It gives an alternative to the numerical modeling scheme, which may be advantageous for fast analysis of different pts/nanoparticle systems. The core of this analytical model is similar to the one presented by Lepeshkevich et al.[40] It provides the time-dependence of singlet oxygen concentration inside and outside the nanospheres in a form of analytical formulae. The spatial distribution of singlet oxygen concentration (which determines the diffusive flux) is not calculated by the analytical model. Instead, the diffusion of singlet oxygen out of the particles is characterized by a single diffusion rate, which is analogous to the escape rate defined by Lepeshkevich et al.[40] The value of this diffusion rate (or the corresponding effective diffusion time) is of major importance. In the work of Lepeshkevich et al.,[40] the experimental results of oxygen rebinding to myoglobin were used to evaluate the mentioned escape rate. This method, however, is not applicable to most of the pts-loaded nanoparticle systems. A semiempirical formula is proposed in this work to calculate the characteristic diffusion time of singlet oxygen based on the particle radius, the diffusion constants of singlet oxygen inside and outside the particles, and the decay rate of singlet oxygen in the surrounding solution. The validity range of the proposed formula is tested by direct comparison between the results of the analytical and numerical models.

THEORETICAL METHODS

Numerical Model. The proposed numerical model calculates the concentration $[\Delta]$ of singlet oxygen produced by photosensitization in spherical particles of radius R (see Figure 1)

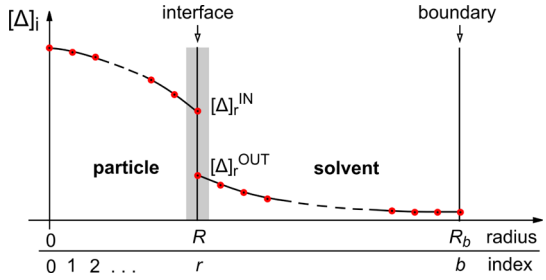

Figure 1. Schematic view of the singlet oxygen spatial distribution inside and outside the nanoparticles as calculated by the numerical model.

by solving the diffusion equation complemented with source and decay terms

$$\frac{\partial[\Delta]}{\partial t} = D\nabla^2([\Delta]) + S - \frac{[\Delta]}{\tau_\Delta} \tag{1}$$

D and τ_Δ are the singlet oxygen diffusion coefficient and lifetime, respectively, both being dependent on the local environment. S is the production rate of singlet oxygen. The diffusion equation is solved numerically in spherical coordinates using a radial grid of equal spacing dr. The corresponding grid point indexes are $i = (0, 1, ..., b)$, where b indicates the boundary of the simulated region located at $R_b = b$ dr. The interface between the particle and the solvent is located at $i = r = R/\mathrm{d}r$. The time derivative is approximated by a forward difference and the corresponding finite difference form of eq 1 is chosen as follows[49]

$$\frac{\mathrm{d}[\Delta]_i}{\mathrm{d}t} = \frac{6D_0([\Delta]_1 - [\Delta]_0)}{(\mathrm{d}r)^2} + S_0 - \frac{[\Delta]_0}{\tau_{\Delta 0}} \qquad \text{for } i = 0 \tag{2}$$

$$\frac{\mathrm{d}[\Delta]_i}{\mathrm{d}t} = \frac{D_i}{2i(\mathrm{d}r)^2}((i+2)[\Delta]_{i+1} - 2i[\Delta]_i + (i-2)[\Delta]_{i-1}) + \frac{D_{i+1}}{2(\mathrm{d}r)^2}([\Delta]_{i+1} - [\Delta]_i) + \frac{D_{i-1}}{2(\mathrm{d}r)^2}([\Delta]_{i-1} - [\Delta]_i) + S_i - \frac{[\Delta]_i}{\tau_{\Delta i}}$$
$$\text{for } i = (1, \ ..., \ r-1) \text{ and } i = (r+1, \ ..., \ b-1) \tag{3}$$

DOI: 10.1021/acs.jpcb.8b00658
J. Phys. Chem. B 2018, 122, 5147−5153

Equation 3 can be used for particles with nonhomogeneous (multi-shell-like) internal structure, where the diffusion coefficient, the source, and the lifetime of singlet oxygen depend on the distance from the particle center.

The source term S_i is proportional to the product of the triplet-state pts and ground-state oxygen concentrations. It is assumed in our model that the ground-state oxygen concentration is not affected by the photodynamic process and stays constant throughout the experiment. The time course of the pts triplet-state concentration can be determined experimentally in a laser-flash photolysis measurement.

The interface between the particle and the surrounding solution (at $i = r$) needs to be treated separately. In general, there is a difference in singlet oxygen concentrations inside and outside the particle, denoted here as $[\Delta]_r^{IN}$ and $[\Delta]_r^{OUT}$ (see Figure 1). The concentration ratio at the interface is defined by the partition coefficient $K = [\Delta]_r^{IN}/[\Delta]_r^{OUT}$. It is assumed in our model that a constant concentration ratio is sustained at all conditions, and this ratio is not affected by the transport of singlet oxygen through the interface. In each time step, the change of the total concentration $[\Delta]_r^{IN} + [\Delta]_r^{OUT}$ is calculated for an interfacial layer of thickness dr (indicated in gray in Figure 1) using the following approximation

$$\frac{d([\Delta]_r^{IN} + [\Delta]_r^{OUT})}{dt} = \frac{1}{r^2\, dr^2}\{D^{IN} r_{IN}^2([\Delta]_{r-1} - [\Delta]_r^{IN}) + D^{OUT} r_{OUT}^2 ([\Delta]_{r+1} - [\Delta]_r^{OUT})\} + \frac{S_r}{2} - \frac{[\Delta]_r^{IN}}{\tau_{\Delta r}^{IN}} - \frac{[\Delta]_r^{OUT}}{\tau_{\Delta r}^{OUT}} \quad (4)$$

where $r_{IN} = r - 0.5$ and $r_{OUT} = r + 0.5$. The two terms inside the curly brackets belong to the flux of singlet oxygen through the inner and the outer surface of the interface layer, the remaining three terms being the source and depletion terms inside the layer. The possible quenching of singlet oxygen molecules located in the solvent (right at the outer surface of the particle) by the particle material is neglected. In each time step, new values of $[\Delta]_r^{IN}$ and $[\Delta]_r^{OUT}$ are calculated, taking the partition condition into account

$$[\Delta]_r^{IN} = \{([\Delta]_r^{IN} + [\Delta]_r^{OUT})_{old} + d([\Delta]_r^{IN} + [\Delta]_r^{OUT})\} \frac{K}{1 + K} \quad (5)$$

$$[\Delta]_r^{OUT} = \frac{[\Delta]_r^{IN}}{K} \quad (6)$$

The outer radius R_b of the simulated area (see Figure 1) is set to the effective diffusion space radius determined by the concentration of simulated nanoparticles n ($R_b^3 = 3/(4\pi n)$). Fully reflecting boundary walls are used (by setting $[\Delta]_b = [\Delta]_{b-1}$) to account for singlet oxygen generated by neighboring nanoparticles. The effects connected to particle motion are neglected.

The model describes the time evolution of singlet oxygen spatial distribution inside and outside the particle. In order to simulate the phosphorescence intensity data, the emission contribution of both singlet oxygen groups (inside and outside the nanoparticle) needs to be taken into account. The phosphorescence signal emitted from a certain volume element is proportional to the local concentration of singlet oxygen and the corresponding rate constant of radiative deactivation k_r. The value of k_r may be different in the particle interior and the surrounding solvent.[40,47] It follows that the overall phosphorescence signal $P(t)$ is proportional to the linear combination of the total amount of singlet oxygen inside and outside the particle and can be approximated as follows

$$P(t) = A(E\Delta_{tot}^{IN} + \Delta_{tot}^{OUT}) \quad (7)$$

where

$$\Delta_{tot}^{IN} = 4\pi\, dr^3\left(\sum_{i=1}^{r-1}[\Delta]_i i^2 + \frac{[\Delta]_r^{IN} r^2}{2} + \frac{[\Delta]_0^{IN}}{24}\right) \quad (8a)$$

$$\Delta_{tot}^{OUT} = 4\pi\, dr^3\left(\sum_{i=r+1}^{b}[\Delta]_i i^2 + \frac{[\Delta]_r^{OUT} r^2}{2}\right) \quad (8b)$$

The emission factor $E = k_r^{IN}/k_r^{OUT}$ is the ratio of the phosphorescence emission rate constants inside and outside the particle (assumed to be a constant for the whole particle interior), and A is a proportionality factor. It is to be noted that the absolute value of the singlet oxygen source term (see eqs 2–4) is usually not known. Because of this fact, only the relative concentration and relative phosphorescence intensity of singlet oxygen can be calculated.

The Analytical Model. In this section, a simplified theoretical approach describing the time course of singlet oxygen total concentration inside and outside the nanoparticles is presented. The scheme of the physical processes taken into account is shown in Figure 2. The model assumptions can be listed as follows. First, singlet oxygen diffusion out of the particles is characterized with a single "effective" diffusion time τ_D^{eff}. It will be shown later that this assumption is well-justified in the case of small particles. Second, the source of singlet oxygen is decaying exponentially, as determined by the pts triplet-state decay time

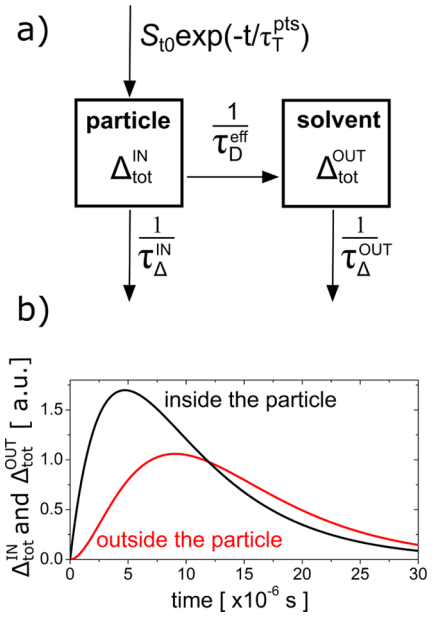

Figure 2. (a) The outline of the analytical model. The source, diffusion, and depletion rates are characterized by the corresponding lifetime values. (b) The characteristic time-dependence of the total amount of singlet oxygen inside and outside a nanoparticle as calculated by eqs 10a and 10b for $\tau_\Delta^{IN} = 10\ \mu s$, $\tau_\Delta^{OUT} = 4\ \mu s$, $\tau_T^{pts} = 7\ \mu s$, and $\tau_D^{eff} = 5\ \mu s$.

DOI: 10.1021/acs.jpcb.8b00658
J. Phys. Chem. B 2018, 122, 5147–5153

τ_T^{pts}. This assumption corresponds to short-pulse photoactivation of the pts. Third, the particle interior is homogeneous with the corresponding singlet oxygen lifetime τ_Δ^{IN}. Similarly, singlet oxygen is deactivated in the surrounding solution at a rate of $1/\tau_\Delta^{OUT}$.

The kinetic equations for the total amount of singlet oxygen inside and outside the nanospheres can be written as follows (see Figure 2a)

$$\frac{d\Delta_{tot}^{IN}}{dt} = S_{t0}\exp\left(-\frac{t}{\tau_T^{pts}}\right) - \Delta_{tot}^{IN}\left(\frac{1}{\tau_\Delta^{IN}} + \frac{1}{\tau_D^{eff}}\right) \quad (9a)$$

$$\frac{d\Delta_{tot}^{OUT}}{dt} = \frac{\Delta_{tot}^{IN}}{\tau_D^{eff}} - \frac{\Delta_{tot}^{OUT}}{\tau_\Delta^{OUT}} \quad (9b)$$

Defining the overall lifetime of singlet oxygen inside the particle τ_p as $1/\tau_p = 1/\tau_\Delta^{IN} + 1/\tau_D^{eff}$, the analytical solution of the coupled differential eqs 9a and 9b has a form

$$\Delta_{tot}^{IN} = \frac{S_{t0}}{\frac{1}{\tau_T^{pts}} - \frac{1}{\tau_p}}\left[\exp\left(-\frac{t}{\tau_p}\right) - \exp\left(-\frac{t}{\tau_T^{pts}}\right)\right] \quad (10a)$$

$$\Delta_{tot}^{OUT} = \frac{S_{t0}}{\tau_D^{eff}\left(\frac{1}{\tau_T^{pts}} - \frac{1}{\tau_p}\right)}\left[\frac{\exp\left(-\frac{t}{\tau_p}\right) - \exp\left(-\frac{t}{\tau_\Delta^{OUT}}\right)}{\frac{1}{\tau_\Delta^{OUT}} - \frac{1}{\tau_p}} - \frac{\exp\left(-\frac{t}{\tau_T^{pts}}\right) - \exp\left(-\frac{t}{\tau_\Delta^{OUT}}\right)}{\frac{1}{\tau_\Delta^{OUT}} - \frac{1}{\tau_T^{pts}}}\right] \quad (10b)$$

The time-dependence of the total singlet oxygen amount inside the particles (see eq 10a and the black curve in Figure 2b) is described by two exponential terms. The shorter lifetime component (τ_p or τ_T^{pts}) belongs to the rising part of the curve, whereas the longer lifetime value determines the exponential decay in the long-time limit. This behavior is analogous to short-pulse singlet oxygen production in homogeneous pts solutions (without nanoparticles).

The time course of the total amount of singlet oxygen outside the particle is described by four exponential terms (combining three different lifetimes, see eq 10b). The general shape of the corresponding curve is shown in Figure 2b (red line). It can be seen that because of the finite diffusion time, the initial rise of singlet oxygen concentration outside the particle is delayed as compared to the concentration rise in the particle interior. In the zero-time limit (right after the excitation pulse), the slope of the singlet oxygen concentration time course outside the particle is zero (no singlet oxygen is produced there). This is different from the time course of the singlet oxygen concentration inside the particle, where the zero-time slope is determined by S_{t0}.

Supposing that the emission factor E and the lifetime values τ_T^{pts}, τ_Δ^{IN}, τ_Δ^{OUT}, and τ_D^{eff} are known, the phosphorescence kinetics of singlet oxygen (as detected in a short-pulse experiment) can be predicted by substituting 10a and 10b into eq 7. The estimation of τ_D^{eff} is of major importance. In general, τ_D^{eff} is affected by the particle diameter R, the diffusion constants of singlet oxygen inside and outside the particle, D^{IN} and D^{OUT}, and the partition coefficient K. Moreover, the diffusion of singlet oxygen out of the particle is faster when singlet oxygen is efficiently depleted in the surrounding solution. As a consequence, one would expect a minor dependence of τ_D^{eff} on τ_Δ^{OUT}, too. To calculate τ_D^{eff}, we propose a semiempirical formula in the following form

$$|\tau_D^{eff}|_{calc} = R^2\left(\frac{1}{7.8\,D_{IN}} + \frac{(K-0.3)Z}{3D_{OUT}(1.3R+Z)}\right) \quad (11)$$

where $Z = \sqrt{D^{OUT}\tau_\Delta^{OUT}}$. Equation 11 can be rationalized as shown in Supporting Information A. It is emphasized that the above relation was derived for homogeneous particles with homogeneously distributed source of singlet oxygen localized solely inside the particles. In real heterogeneous systems, site-dependent (multiexponential) pts triplet-state kinetics may occur,[38] the treatment of which is beyond the scope of the present analytical model. The numerical constants of eq 11 were optimized to get a good match between the numerical and analytical models (see the Results and Discussion section). As a consequence, the limitations of the numerical model are transmitted to this formula, too. For example, the possible quenching of singlet oxygen molecules located right at the particle surface (but still outside the particle) by the particle constituents was not taken into account. Because of this fact, in order to keep the two models self-consistent, the lifetime of singlet oxygen in the pure solvent is to be used for τ_Δ^{OUT} when calculating the Z value.

Test Conditions for Simulation Studies. The kinetics of singlet oxygen concentration produced in spherical nanoparticles was followed by running the simulations on a homogeneous particle model. It was assumed in these studies that the particles are of no internal structure and that singlet oxygen is equally produced in the entire particle volume. An exponentially decaying source term was applied to mimic the pts triplet-state decay in a pulsed laser experiment. These assumptions allow for direct comparison between the numerical and analytical results. The particle radius was varied in the range of 4−200 nm. It was our goal to cover the transition from small particles to large ones. In the case of small particles, singlet oxygen diffuses out to the surroundings in a very short time compared to singlet oxygen and pts triplet-state lifetimes. By contrast, in large particles, the diffusion time may exceed the lifetimes of singlet oxygen and pts triplet-state decay. The outer radius of the simulated region was increased proportionally to the particle size, keeping a constant value of $R_b/R = 16$. This ratio was tested to be large enough not to affect the computational results significantly, even in the case of the smallest particles studied. It follows that the studied conditions belong to the low particle concentration limit.

For the sake of simplicity, the lifetime of singlet oxygen inside and outside the particle and the pts triplet-state lifetime were kept constant, choosing a realistic set of lifetime values: $\tau_\Delta^{IN} = 10$ μs, $\tau_\Delta^{OUT} = 4$ μs, and $\tau_T^{pts} = 7$ μs. The remaining parameters were varied in the following ranges: $D^{IN} = (0.2-1.0) \times 10^{-9}$ m^2 s^{-1}, $D^{OUT} = (1.0-4.0) \times 10^{-9}$ m^2 s^{-1}, and $K = (1-4)$. The time step of the numerical simulations was set to $dt = 2.5 \times 10^{-13}$ s. The spatial grid spacing was $dr = 0.2$ nm, for $R = 4$ nm particles, and increased up to $dr = 10$ nm for $R = 200$ nm particles. Smaller dr and dt values did not change the numerical results significantly.

RESULTS AND DISCUSSION

Spatiotemporal Concentration Distribution of Singlet Oxygen. The numerical model was used to calculate the time evolution of singlet oxygen spatial distribution inside and outside the nanoparticles using the parameter set described above. Typical results obtained for particles with 60 nm radius are

DOI: 10.1021/acs.jpcb.8b00658
J. Phys. Chem. B 2018, 122, 5147−5153

shown in Figure 3. It can be seen that during the first 4 μs, the concentration of singlet oxygen increases inside the particle. At

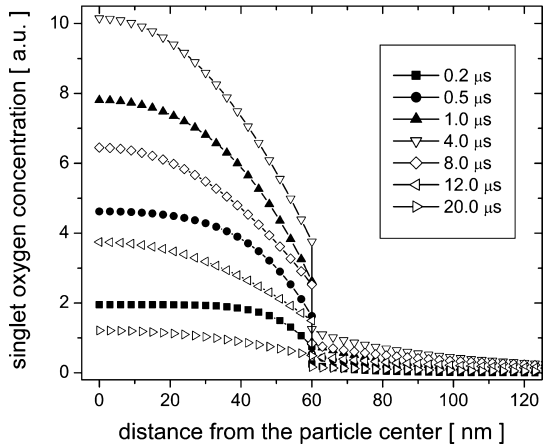

Figure 3. The spatial distribution of singlet oxygen concentration at different times after pts photoactivation calculated by the numerical model. The simulation parameters are R = 60 nm, D^{IN} = 0.5×10^{-9} m^2 s^{-1}, D^{OUT} = 2.0×10^{-9} m^2 s^{-1}, K = 3, τ_Δ^{IN} = 10 μs, τ_Δ^{OUT} = 4 μs, and τ_T^{pts} = 7 μs.

the same time, the shape of the distribution gradually changes from a (predominantly) flat curve to a parabolic radial dependence. After reaching the maximum, the concentration starts to decrease.

It is important to note that depending on the experimental conditions, the total number of singlet oxygen molecules inside a single particle (at a certain time) may be extremely low. For example, the average number of oxygen molecules inside the particles with 10 nm diameter in aqueous environment at air-saturated conditions can be as low as 2−3 pieces. This number was estimated from the oxygen-solubility data[50] using a partition coefficient of K = 3 for the particle/water environment. It is unlikely that the number of singlet oxygen molecules would exceed the (equilibrated) number of ground-state oxygen molecules dramatically in the particle interior at any condition. As a consequence, the calculated spatial distribution (as shown in Figure 3) should be viewed as an average distribution in a large-particle ensemble.

Comparison of the Numerical and Analytical Models. The total amount of singlet oxygen inside and outside the particles is plotted in Figures 4a and 4b for nanoparticles of R = 20 nm and R = 200 nm radius, respectively. The results of the numerical model (see eqs 8a and 8b) are indicated with open symbols, and the solid lines belong to the analytical solution (eqs 10a and 10b). In the case of the smaller (20 nm radius) particle, singlet oxygen, after being produced inside the particle, diffuses out to the surrounding solution very fast. Because of this fact, the overall singlet oxygen concentration outside the particle exceeds the interior concentration (except for the very first microsecond). The opposite situation applies for large particles, where only a small portion of singlet oxygen diffuses out to the solution.

As mentioned in the Theoretical Methods section, the analytical model relies on the knowledge of the effective diffusion time τ_D^{eff}. In the present work, this parameter was determined in two ways. First, the diffusion time was used as a fitting parameter to find the best match between the analytical and numerical results. The details of the fitting procedure are described in Supporting Information B. The obtained diffusion time is

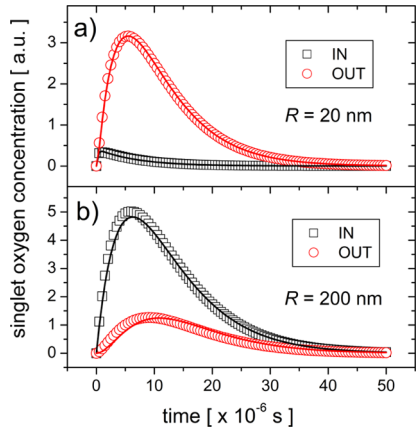

Figure 4. The time course of the total (integrated) singlet oxygen concentration inside and outside the nanoparticles as calculated for (a) R = 20 nm and (b) R = 200 nm particles. The open symbols represent the results of the numerical model. The solid lines indicate the best fit of the analytical model to the numerical data. Simulation parameters: D^{IN} = 0.5×10^{-9} m^2 s^{-1}, D^{OUT} = 2.0×10^{-9} m^2 s^{-1}, K = 3, τ_Δ^{IN} = 10 μs, τ_Δ^{OUT} = 4 μs, and τ_T^{pts} = 7 μs.

denoted as $|\tau_D^{eff}|_{fitted}$. The solid lines plotted in Figure 4 represent such fitted analytical solutions. Evidently, the numerical results are well-described by the analytical model in the case of small particles (Figure 4a), and a reasonable agreement of the numerical and analytical results is found in the case of large particles (Figure 4b).

The effective diffusion time (denoted as $|\tau_D^{eff}|_{calc}$) was also calculated from eq 11. The validity and applicability of the proposed formula was tested by direct comparison of $|\tau_D^{eff}|_{calc}$ and $|\tau_D^{eff}|_{fitted}$ at different conditions. The results are shown in Figure 5a as a function of the partition coefficient K (for different D^{IN} values) and in Figure 5b as a function of the particle radius R (for different D^{OUT} values). It is obvious that in the studied range of parameters, the values of $|\tau_D^{eff}|_{calc}$ obtained from eq 11 are almost identical to $|\tau_D^{eff}|_{fitted}$, which provide the best fit of the analytical model to the numerical results. The diffusion time is a linear function of the partition coefficient K (Figure 5a) and for small particles it scales with the square of the particle radius (Figure 5b).

CONCLUSIONS

The phosphorescence kinetics of singlet oxygen produced by photosensitization of pts in nanoparticles is affected by the diffusion of singlet oxygen from the particle interior to the surrounding solvent. The time course of the phosphorescence signal generated with short-pulse (few nanosecond or sub-nanosecond range) excitation depends on various physical parameters including the particle size, the diffusion coefficients, and singlet oxygen lifetimes both inside and outside the particles, the lifetime of the photosensitizer triplet state, the oxygen partition coefficient for the given particle/solvent system, and the emission factor, that is, the ratio of the rate constants for singlet oxygen radiative decay inside and outside the particle.

The two theoretical models presented in this work predict the phosphorescence kinetics of singlet oxygen in the near-infrared region (around 1270 nm) following pulsed excitation of the pts molecules encapsulated inside the spherical particles. The numerical model solves the singlet oxygen diffusion equation on a one-dimensional radial grid and gives information on the spatiotemporal distribution of singlet oxygen concentration both

DOI: 10.1021/acs.jpcb.8b00658
J. Phys. Chem. B 2018, 122, 5147−5153

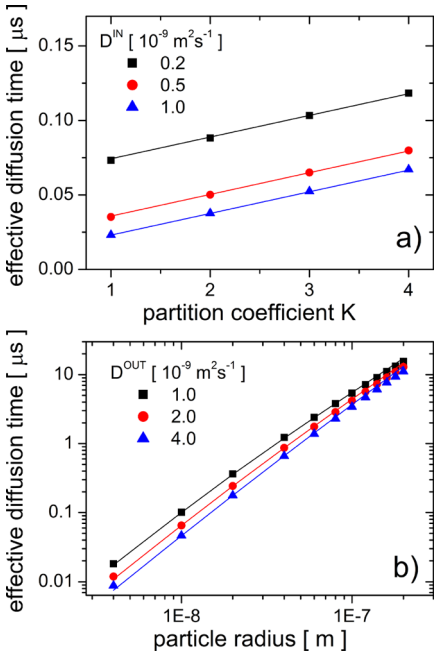

Figure 5. The effective diffusion time plotted (a) as a function of the partition coefficient K for different D^{IN} values (R = 10 nm, $D^{OUT} = 2.0 \times 10^{-9}$ m^2 s^{-1}) and (b) as a function of the particle radius R for different D^{OUT} values ($K = 3$, $D^{IN} = 0.5 \times 10^{-9}$ m^2 s^{-1}). The remaining parameters are $\tau_\Delta^{IN} = 10$ μs, $\tau_\Delta^{OUT} = 4$ μs, and $\tau_T^{pts} = 7$ μs. The solid symbols represent $|\tau_D^{eff}|_{fitted}$, obtained by fitting the analytical model to the numerical results. The lines belong to $|\tau_D^{eff}|_{calc}$ calculated from eq 11.

inside and outside the particles. The corresponding phosphorescence signal can be obtained by linear combination of the total (integrated) singlet oxygen concentrations in the particle interior and exterior, taking the emission factor into account.

As it may be time-consuming to set up and run the numerical code, an analytical model was also presented. This simplified model can be used for fast analysis of studied nanoparticle/pts systems. An analytical formula was proposed to calculate the diffusion time of singlet oxygen from the particle to the solvent, which can be combined with the analytical solution of rate equations (for singlet oxygen concentrations) to estimate the total (integrated) concentration of singlet oxygen inside and outside the particles. In the first approximation, the diffusion time scales with the square of the particle radius. As a consequence, the size of the nanoparticles plays a key role in the PDT-related delivery systems to ensure high singlet oxygen concentration outside the particles.

In general, one needs to be cautious when interpreting the experimental phosphorescence kinetics data of singlet oxygen produced by photosensitization in nanoparticles. The two models presented in this work facilitate the analysis of measured phosphorescence signals and thus contribute to the development of the PDT-related nanocarrier/pts formulations.

■ ASSOCIATED CONTENT

Supporting Information

The Supporting Information is available free of charge on the ACS Publications website at DOI: 10.1021/acs.jpcb.8b00658.

A: Derivation of the semiempirical formula for the diffusion time $|\tau_D^{eff}|_{calc}$ (eq 11). B: Explanation of the mathematical procedure used to calculate $|\tau_D^{eff}|_{fitted}$ by fitting the analytical model to the numerical results (PDF)

■ AUTHOR INFORMATION

Corresponding Author

*E-mail: gregor.bano@upjs.sk. Phone: +421 55 2342253.

ORCID

Sergei G. Kruglik: 0000-0002-2945-3092
Daniel Jancura: 0000-0003-1968-8709
Gregor Bánó: 0000-0002-8807-2118

Notes

The authors declare no competing financial interest.

■ ACKNOWLEDGMENTS

This work was supported by the APVV-15-0485 grant of the Slovak Ministry of Education and the projects (ITMS codes: 26220120040 and 26220120039) of the Operation Program Research and Development funded by the European Regional Development Fund.

■ REFERENCES

(1) Dolmans, D. E. J. G. J.; Fukumura, D.; Jain, R. K. Photodynamic Therapy for Cancer. *Nat. Rev. Cancer* **2003**, *3*, 380−387.

(2) Robertson, C. A.; Evans, D. H.; Abrahamse, H. Photodynamic Therapy (PDT): A Short Review on Cellular Mechanisms and Cancer Research Applications for PDT. *J. Photochem. Photobiol., B* **2009**, *96*, 1−8.

(3) Ogilby, P. R. Singlet Oxygen: There Is Indeed Something New Under the Sun. *Chem. Soc. Rev.* **2010**, *39*, 3181−3209.

(4) Li, B.; Lin, L.; Lin, H.; Wilson, B. C. Photosensitized Singlet Oxygen Generation and Detection: Recent Advances and Future Perspectives in Cancer Photodynamic Therapy. *J. Biophotonics* **2016**, *9*, 1314−1325.

(5) Krasnovsky, A. A. Luminescence and Photochemical Studies of Singlet Oxygen Photonics. *J. Photochem. Photobiol., A* **2008**, *196*, 210−218.

(6) Schlothauer, J.; Hackbarth, S.; Röder, B. A New Benchmark for Time-Resolved Detection of Singlet Oxygen Luminescence - Revealing the Evolution of Lifetime in Living Cells with Low Dose Illumination. *Laser Phys. Lett.* **2009**, *6*, 216−221.

(7) Niedre, M.; Patterson, M. S.; Wilson, B. C. Direct Near-Infrared Luminescence Detection of Singlet Oxygen Generated by Photodynamic Therapy in Cells in Vitro and Tissues In Vivo. *Photochem. Photobiol.* **2002**, *75*, 382−391.

(8) Jiménez-Banzo, A.; Ragàs, X.; Kapusta, P.; Nonell, S. Time-Resolved Methods in Biophysics. 7. Photon Counting vs. Analog Time-Resolved Singlet Oxygen Phosphorescence Detection. *Photochem. Photobiol. Sci.* **2008**, *7*, 1003−1010.

(9) Kuimova, M. K.; Botchway, S. W.; Parker, A. W.; Balaz, M.; Collins, H. A.; Anderson, H. L.; Suhling, K.; Ogilby, P. R. Imaging Intracellular Viscosity of a Single Cell During Photoinduced Cell Death. *Nat. Chem.* **2009**, *1*, 69−73.

(10) Scholz, M.; Biehl, A.-L.; Dědic, R.; Hála, J. The Singlet-Oxygen-Sensitized Delayed Fluorescence in Mammalian Cells: a Time-Resolved Microscopy Approach. *Photochem. Photobiol. Sci.* **2015**, *14*, 700−713.

(11) Jarvi, M. T.; Niedre, M. J.; Patterson, M. S.; Wilson, B. C. Singlet Oxygen Luminescence Dosimetry (SOLD) for Photodynamic Therapy: Current Status, Challenges and Future Prospects. *Photochem. Photobiol.* **2006**, *82*, 1198−1210.

(12) Pimenta, F. M.; Jensen, R. L.; Holmegaard, L.; Esipova, T. V.; Westberg, M.; Breitenbach, T.; Ogilby, P. R. Singlet-Oxygen-Mediated Cell Death Using Spatially-Localized Two-Photon Excitation of an Extracellular Sensitizer. *J. Phys. Chem. B* **2012**, *116*, 10234−10246.

(13) da Silva, E. F. F.; Pedersen, B. W.; Breitenbach, T.; Toftegaard, R.; Kuimova, M. K.; Arnaut, L. G.; Ogilby, P. R. Irradiation- and Sensitizer-Dependent Changes in the Lifetime of Intracellular Singlet Oxygen Produced in a Photosensitized Process. *J. Phys. Chem. B* **2012**, *116*, 445−461.

DOI: 10.1021/acs.jpcb.8b00658
J. Phys. Chem. B 2018, 122, 5147−5153

(14) Kuimova, M. K.; Yahioglu, G.; Ogilby, P. R. Singlet Oxygen in a Cell: Spatially Dependent Lifetimes and Quenching Rate Constants. *J. Am. Chem. Soc.* **2009**, *131*, 332−340.
(15) Bechet, D.; Couleaud, P.; Frochot, C.; Viriot, M.-L.; Guillemin, F.; Barberi-Heyob, M. Nanoparticles as Vehicles for Delivery of Photodynamic Therapy Agents. *Trends Biotechnol.* **2008**, *26*, 612−621.
(16) Boix-Garriga, E.; Acedo, P.; Casadó, A.; Villanueva, A.; Stockert, J. C.; Cañete, M.; Mora, M.; Sagristá, M. L.; Nonell, S. Poly(D, L-lactide-co-glycolide) Nanoparticles as Delivery Agents for Photodynamic Therapy: Enhancing Singlet Oxygen Release and Phototoxicity by Surface PEG Coating. *Nanotechnology* **2015**, *26*, 365104.
(17) Bhattacharyya, S.; Barman, M. K.; Baidya, A.; Patra, A. Singlet Oxygen Generation from Polymer Nanoparticles-Photosensitizer Conjugates Using FRET Cascade. *J. Phys. Chem. C* **2014**, *118*, 9733−9740.
(18) Li, S.; Chang, K.; Sun, K.; Tang, Y.; Cui, N.; Wang, Y.; Qin, W.; Xu, H.; Wu, C. Amplified Singlet Oxygen Generation in Semiconductor Polymer Dots for Photodynamic Cancer Therapy. *ACS Appl. Mater. Interfaces* **2016**, *8*, 3624−3634.
(19) Chen, C.-Y.; Tian, Y.; Cheng, Y.-J.; Young, A. C.; Ka, J.-W.; Jen, A. K.-Y. Two-Photon Absorbing Block Copolymer as a Nanocarrier for Porphyrin: Energy Transfer and Singlet Oxygen Generation in Micellar Aqueous Solution. *J. Am. Chem. Soc.* **2007**, *129*, 7220.
(20) Kumari, P.; Jain, S.; Ghosh, B.; Zorin, V.; Biswas, S. Polylactide-Based Block Copolymeric Micelles Loaded with Chlorin e6 for Photodynamic Therapy: In Vitro Evaluation in Monolayer and 3D Spheroid Models. *Mol. Pharm.* **2017**, *14*, 3789−3800.
(21) Gibot, L.; Lemelle, A.; Till, U.; Moukarzel, B.; Mingotaud, A.-F.; Pimienta, V.; Saint-Aguet, P.; Rols, M.-P.; Gaucher, M.; Violleau, F.; Chassenieux, C.; Vicendo, P. Polymeric Micelles Encapsulating Photosensitizer: Structure/Photodynamic Therapy Efficiency Relation. *Biomacromolecules* **2014**, *15*, 1443−1455.
(22) Jeong, H.; Huh, M.; Lee, S. J.; Koo, H.; Kwon, I. C.; Jeong, S. Y.; Kim, K. Photosensitizer-Conjugated Human Serum Albumin Nanoparticles for Effective Photodynamic Therapy. *Theranostics* **2011**, *1*, 230−239.
(23) Couleaud, P.; Morosini, V.; Frochot, C.; Richeter, S.; Raehm, L.; Durand, J.-O. Silica-Based Nanoparticles for Photodynamic Therapy Applications. *Nanoscale* **2010**, *2*, 1083−1095.
(24) Rossi, L. M.; Silva, P. R.; Vono, L. L. R.; Fernandes, A. U.; Tada, D. B.; Baptista, M. S. Protoporphyrin IX Nanoparticle Carrier: Preparation, Optical Properties, and Singlet Oxygen Generation. *Langmuir* **2008**, *24*, 12534−12538.
(25) Ma, X.; Qu, Q.; Zhao, Y. Targeted Delivery of 5-Aminolevulinic Acid by Multifunctional Hollow Mesoporous Silica Nanoparticles for Photodynamic Skin Cancer Therapy. *ACS Appl. Mater. Interfaces* **2015**, *7*, 10671−10676.
(26) Wang, J.; Zhong, Y.; Wang, X.; Yang, W.; Bai, F.; Zhang, B.; Alarid, L.; Bian, K. F.; Fan, H. pH-Dependent Assembly of Porphyrin-Silica Nanocomposites and Their Application in Targeted Photodynamic Therapy. *Nano Lett.* **2017**, *17*, 6916−6921.
(27) Chan, M.-H.; Chen, S.-P.; Chen, C.-W.; Chan, Y.-C.; Lin, R. J.; Tsai, D. P.; Hsiao, M.; Chung, R.-J.; Chen, X.; Liu, R.-S. Single 808 nm Laser Treatment Comprising Photothermal and Photodynamic Therapies by Using Gold Nanorods Hybrid Upconversion Particles. *J. Phys. Chem. C* **2018**, *122*, 2402.
(28) Jin, C. S.; Zheng, G. Liposomal Nanostructures for Photosensitizer Delivery. *Lasers Surg. Med.* **2011**, *43*, 734−748.
(29) Derycke, A. S. L.; de Witte, P. A. M. Liposomes for Photodynamic Therapy. *Adv. Drug Delivery Rev.* **2004**, *56*, 17−30.
(30) Konan, Y. N.; Gurny, R.; Allémann, E. State of the Art in the Delivery of Photosensitizers for Photodynamic Therapy. *J. Photochem. Photobiol., B* **2002**, *66*, 89−106.
(31) Reddi, E. Role of Delivery Vehicles for Photosensitizers in the Photodynamic Therapy of Tumours. *J. Photochem. Photobiol., B* **1997**, *37*, 189−195.
(32) Sharman, W. M.; van Lier, J. E.; Allen, C. M. Targeted Photodynamic Therapy via Receptor Mediated Delivery Systems. *Adv. Drug Delivery Rev.* **2004**, *56*, 53−76.
(33) Goto, P. L.; Siqueira-Moura, M. P.; Tedesco, A. C. Application of Aluminum Chloride Phthalocyanine-Loaded Solid Lipid Nanoparticles for Photodynamic Inactivation of Melanoma Cells. *Int. J. Pharm.* **2017**, *518*, 228−241.
(34) Robinson-Duggon, J.; Pérez-Mora, F.; Valverde-Vásquez, L.; Cortés-Arriagada, D.; De la Fuente, J. R.; Günther, G.; Fuentealba, D. Supramolecular Reversible On-Off Switch for Singlet Oxygen Using Cucurbit n uril Inclusion Complexes. *J. Phys. Chem. C* **2017**, *121*, 21782−21789.
(35) Wang, X.-Q.; Lei, Q.; Zhu, J.-Y.; Wang, W.-J.; Cheng, Q.; Gao, F.; Sun, Y.-X.; Zhang, X.-Z. Cucurbit 8 uril Regulated Activatable Supramolecular Photosensitizer for Targeted Cancer Imaging and Photodynamic Therapy. *ACS Appl. Mater. Interfaces* **2016**, *8*, 22892−22899.
(36) Westberg, M.; Holmegaard, L.; Pimenta, F. M.; Etzerodt, M.; Ogilby, P. R. Rational Design of an Efficient, Genetically Encodable, Protein-Encased Singlet Oxygen Photosensitizer. *J. Am. Chem. Soc.* **2015**, *137*, 1632−1642.
(37) Ruiz-González, R.; Cortajarena, A. L.; Mejias, S. H.; Agut, M.; Nonell, S.; Flors, C. Singlet Oxygen Generation by the Genetically Encoded Tag miniSOG. *J. Am. Chem. Soc.* **2013**, *135*, 9564−9567.
(38) Westberg, M.; Bregnhøj, M.; Etzerodt, M.; Ogilby, P. R. Temperature Sensitive Singlet Oxygen Photosensitization by LOV-Derived Fluorescent Flavoproteins. *J. Phys. Chem. B* **2017**, *121*, 2561−2574.
(39) Westberg, M.; Bregnhøj, M.; Etzerodt, M.; Ogilby, P. R. No Photon Wasted: An Efficient and Selective Singlet Oxygen Photosensitizing Protein. *J. Phys. Chem. B* **2017**, *121*, 9366−9371.
(40) Lepeshkevich, S. V.; Parkhats, M. V.; Stasheuski, A. S.; Britikov, V. V.; Jarnikova, E. S.; Usanov, S. A.; Dzhagarov, B. M. Photosensitized Singlet Oxygen Luminescence from the Protein Matrix of Zn-Substituted Myoglobin. *J. Phys. Chem. A* **2014**, *118*, 1864−1878.
(41) Wilkinson, F.; Helman, W. P.; Ross, A. B. Rate Constants for the Decay and Reactions of the Lowest Electronically Excited Singlet-State of Molecular-Oxygen in Solution - an Expanded and Revised Compilation. *J. Phys. Chem. Ref. Data* **1995**, *24*, 663−1021.
(42) Scurlock, R. D.; Nonell, S.; Braslavsky, S. E.; Ogilby, P. R. Effect of Solvent on the Radiative Decay of Singlet Molecular-Oxygen (A(1)-Delta(G)). *J. Phys. Chem.* **1995**, *99*, 3521−3526.
(43) Bregnhøj, M.; Westberg, M.; Jensen, F.; Ogilby, P. R. Solvent-Dependent Singlet Oxygen Lifetimes: Temperature Effects Implicate Tunneling and Charge-Transfer Interactions. *Phys. Chem. Chem. Phys.* **2016**, *18*, 22946−22961.
(44) Bregnhøj, M.; Westberg, M.; Minaev, B. F.; Ogilby, P. R. Singlet Oxygen Photophysics in Liquid Solvents: Converging on a Unified Picture. *Acc. Chem. Res.* **2017**, *50*, 1920−1927.
(45) Poulsen, L.; Zebger, I.; Tofte, P.; Klinger, M.; Hassager, O.; Ogilby, P. R. Oxygen Diffusion in Bilayer Polymer Films. *J. Phys. Chem. B* **2003**, *107*, 13885−13891.
(46) Zebger, I.; Poulsen, L.; Gao, Z.; Andersen, L. K.; Ogilby, P. R. Singlet Oxygen Images of Heterogeneous Samples: Examining the Effect of Singlet Oxygen Diffusion Across the Interfacial Boundary in Phase-Separated Liquids and Polymers. *Langmuir* **2003**, *19*, 8927−8933.
(47) Hackbarth, S.; Röder, B. Singlet Oxygen Luminescence Kinetics in a Heterogeneous Environment - Identification of the Photosensitizer Localization in Small Unilamellar Vesicles. *Photochem. Photobiol. Sci.* **2015**, *14*, 329−334.
(48) Hackbarth, S.; Schlothauer, J.; Preuß, A.; Röder, B. New Insights to Primary Photodynamic Effects - Singlet Oxygen Kinetics in Living Cells. *J. Photochem. Photobiol., B* **2010**, *98*, 173−179.
(49) Versypt, A. N. F.; Braatz, R. D. Analysis of Finite Difference Discretization Schemes for Diffusion in Spheres with Variable Diffusivity. *Comput. Chem. Eng.* **2014**, *71*, 241−252.
(50) Geng, M.; Duan, Z. Prediction of Oxygen Solubility in Pure Water and Brines up to High Temperatures and Pressures. *Geochim. Cosmochim. Acta* **2010**, *74*, 5631−5640.

DOI: 10.1021/acs.jpcb.8b00658
J. Phys. Chem. B 2018, 122, 5147−5153